A dual-responsive "*turn-on*" bifunctional receptor: chemosensor for Fe^{3+} and chemodosimeter for Hg^{2+}

Sujay Mukhopadhyay[a], Rakesh Kumar Gupta[a], Arnab Biswas[a], Amit Kumar[a], Mrigendra Dubey[a], Maninder Singh Hundal[b] and Daya Shankar Pandey*[a]

[a]Department of Chemistry, Faculty of Science, Banaras Hindu University, Varanasi - 221 005 (U.P.) India

[b]Department of Chemistry, Guru Nanak Dev University, Amritsar- 143005 (Punjab), India

Contents

General Information

Materials and methods

The solvents were dried and distilled by standard literature procedures prior to their use.[1] Metal nitrates viz., $NaNO_3$, KNO_3, $Ca(NO_3)_2{\cdot}4H_2O$, $Mg(NO_3)_2{\cdot}6H_2O$, $Co(NO_3)_2{\cdot}6H_2O$, $Ni(NO_3)_2{\cdot}6H_2O$, $Cu(NO_3)_2{\cdot}3H_2O$, $Zn(NO_3)_2{\cdot}6H_2O$, $Cd(NO_3)_2{\cdot}4H_2O$, $AgNO_3$, $Pb(NO_3)_2$, $Hg(NO_3)_2$, and $Fe(NO_3)_3.9H_2O$ were obtained from *s d fine-chem limited*, Mumbai, India and 2-aminophenyl benzimidazole, *p*-anisidine, *p*-tolludine, acetanilide were procured from Sigma-Aldrich chemicals pvt. Ltd. and were used without further purification.

Instrumental details

Elemental analyses for C, H, and N were performed on an Exeter Analytical Inc. model CE-440 CHN analyzer. IR and electronic absorption spectra (50% aqueous-acetonitrile) were acquired on a PerkinElmer Spectrum Version Varian 3300 FT-IR, and Shimadzu UV-1601 Spectrometers, respectively. Fluorescence spectra (50% aqueous-acetonitrile) were acquired at room temperature on a PerkinElmer *LS 55* Fluorescence Spectrometer, the excitation and emission slit widths were set at 10.0 and 2.5 nm, respectively. ^1H (300 MHz) and ^{13}C (75.45 MHz) NMR spectra at rt were obtained on a JEOL AL300 FT-NMR Spectrometer using tetramethylsilane [$Si(CH_3)_4$] as an internal reference. Electrospray ionization mass spectrometric (ESI-MS) measurements were made on a Bruker Dalton-ics Amazon SL ion trap mass spectrometer. Samples were dissolved in 100% acetonitrile with 0.1% formic acid and introduced into the ESI source through a syringe pump at a flow rate of 100 μL/h. The capillary voltage was at 4500V, dry gas flow at 8 L/min, and dry gas at 300 °C. The MS scan was acquired for 2.0 min and spectra print outs were averaged of over each scan.

X-ray Structure Determination.

Crystals suitable for X-ray single crystal analyses for **L1**, **L2** and **L3** were obtained by slow diffusion of methanol over a dichloromethane solution of the respective compounds. X-ray data on these compounds were collected on a Bruker Kappa Apex-II Diffractometer at RT with Mo-Kα radiation (λ = 0.71073 Å) at Department of Chemistry, Centre for Advanced Studies, Guru Nanak Dev University, Amritsar, India. Structures were solved by direct methods (SHELXS 97) and refined by full-matrix least squares on F^2 (SHELX 97).[2] All the

non-H atoms were treated anisotropically. H-atoms attached to the carbon were included as fixed contribution and geometrically calculated and refined using SHELX riding model. Computer program PLATON was used for analyzing interaction and stacking distances.[3] CCDC deposition Nos. 1034021, 1034019, 1034022 (**L1**, **L2** and **L3**) and 1034020 (**CMQC**) contains the supplementary crystallographic data for this paper. The data can be obtained free of charge *via* http://www.ccdc.cam.ac.uk/conts/retrieving html (or from the CCDC, 12 Union Road, Cambridge CB2 1EZ, UK; Fax: +44-1223-336033; E-mail: deposit@ccdc.cam.ac.uk).

General method of UV–vis and fluorescence titration

Spectroscopic properties of **L1**, **L2**, **L3, L1**–Fe^{3+}, and **L1**–Hg^{2+} were investigated by monitoring absorption and fluorescence changes by addition of the nitrate salts of cations in water, including Na^{+}, K^{+}, Ca^{2+}, Mg^{2+}, Al^{3+}, Cu^{2+}, Ag^{+}, Cr^{3+}, Mn^{2+}, Co^{2+}, Ni^{2+}, Fe^{3+}, Zn^{2+}, Cd^{2+} and Hg^{2+}. The excitation wavelengths for all the fluorescence experiments are chosen with respect to the absorbance maxima of probes and the λ_{ex} are kept constant in the total fluorescence titration experiments and no correction for the absorbed light was made.

Calculation of limit of detection (LOD)

Quantitative responses of **L1**, **L2**, **L3** toward Fe^{3+} and Hg^{2+} were investigated using linear calibration plots from fluorescence spectral studies. Dynamic range for determination of LOD for these ions has been found to be linear. The LOD has been evaluated using $3\sigma/s$, where σ is the standard deviation of the blank signals and s is the slope of the linear calibration plot.

Theoretical Calculations

Molecular structure of **L1**–Fe^{3+} was designed using ChemBioDraw Ultra software and 3D views of the structures were optimized by minimizing energy of the molecule using MM2 mode using the same software. Optimization and energy calculations were performed on Gaussian09 with a density functional theory (DFT) in the B3LYP mode in the ground state.[4-5] The basis set 6-31G(d,p) has been used for all the light atoms (C, H , N, O), while LANL2DZ for the metal atom (Fe) with an effective-core pseudo-potential.[6]

Syntheses of the L1-L3.

2-chloro-3-formylquinoline and its methyl and methoxy derivatives were prepared following literature procedures.[7]

Synthesis of L1.

2-aminophenylbenzimidazole (209 mg, 1 mmol) was added to a hot ethanolic solution of 2-chloro-3-formyl-7-methoxyquinoline (221 mg, 1 mmol) and the contents of the flask were refluxed for 4 hours. Upon cooling to room temperature it afforded a pale yellow precipitate which was filtered and washed with diethyl ether. It was further dissolved in DCM and layered with methanol to give yellow brown crystals. Yield: 93.5% (0.385 g). Anal. Calc for $C_{24}H_{17}ClN_4O$, requires: C, 69.82; H, 4.15; N, 13.57%. Found C, 69.67; H, 4.06; N, 13.43%. IR (KBr pellets, cm^{-1}): 462, 728, 743, 1036, 1165, 1165, 1259, 1318, 1330, 1453, 1496, 1508, 1618, 2925.^{1}H NMR (DMSO d_6, δ ppm): 3.89 (s, 3H, OC$\underline{H_3}$); 6.84 (t, 3H, phenyl); 7.01 (t, 1H, phenyl), 7.20 (m, 5H, phenyl), 7.46 (t, 1H, phenyl), 7.68 (d, 1H, phenyl), 7.82 (d, 1H, phenyl), 8.01 (t, 2H, phenyl). ^{13}C NMR (DMSO d_6, δ ppm): 55.75, (O$\underline{C}H_3$), 106.29, 111.05,114.79, 118.59, 121.49, 122.39, 124.72, 127.49, 129.58, 132.11, 137.08, 143.19, 148.10, 161.95($\underline{C_6}H_6$). ESI-MS. (Calcd, found, *m*/*z*): $[M + H]^+$ 413.1169, 413.1167.

Synthesis of L2.

The probe **L2** was prepared by the above procedure adapted for synthesis of **L1** using 2-chloro-3-formyl-6-methylquinoline (205 mg, 1 mmol**)**. Orange yellow colored crystals were obtained in excellent yield. Yield: 92.2% (0.365 g). Anal. Calc for 143.19, $C_{24}H_{17}ClN_4$, requires: C, 72.63; H, 4.32; N, 14.12%. Found C, 72.53; H, 4.26; N, 14.07%. IR (KBr pellets, cm^{-1}): 553, 572, 818, 844, 954, 1013, 1171, 1359, 1410, 1504, 1625, 2227, 2867, 2962.^{1}H NMR (DMSO d_6, δ ppm): 2.36 (s, 3H, C$\underline{H_3}$); 6.85 (q, 2H, phenyl); 6.98 (t, 2H, phenyl), 7.04 (d, 2H, phenyl), 7.20 (m, 1H, phenyl), 7.56 (d, 2H, phenyl), 7.71 (t, 2H, phenyl), 7.83 (d, 1H, phenyl), 8.03 (d, 1H, phenyl). ^{13}C NMR (DMSO d_6, δ ppm): 20.91, ($\underline{C}H_3$); 110.8, 115.04, 118.61, 122.49, 123.40, 126.87, 130.01, 132.98, 136.99, 142.15, 143.95, 145.44, 146.99($\underline{C_6}H_6$). ESI-MS. (Calcd, found, *m*/*z*): $[M + H]^+$ 397.1220, 397.1223.

Synthesis of L3.

It was synthesized following the above procedure adapted for **L1** except that 2-chloro-3-formyl-6-quinoline (191 mg, 1 mmol**)** was used in place of 2-chloro-3-formyl-7-

methoxyquinoline. Yellow color crystals were obtained. Yield: 93.4% (0.357 g). Anal. Calc for $C_{23}H_{15}ClN_4$, requires: C, 72.16; H, 3.95; N, 14.63%. Found C, 72.08; H, 4.08; N, 14.56%. IR (KBr pellets, cm^{-1}): 461, 487, 597, 744, 1030, 1264, 1306, 1330, 1388, 1452, 1491, 1617, 2933, 2962.^{1}H NMR (DMSO d_6, δ ppm): 6.84 (t, 2H, Ph); 6.94 (d, 1H, Ph), 7.03 (t, 1H, Ph), 7.20 (m, 2H, phenyl), 7.58 (q, 2H, phenyl), 7.65 (d, 1H, phenyl), 7.77 (t, 1H, phenyl), 8.00 (m, 4H, phenyl). ^{13}C NMR (DMSO d_6, δ ppm): 110.14, 111.37, 114.96, 118.61, 122.42, 124.71, 126.43, 127.97, 130.08, 132.23, 137.12, 142.20, 143.95, 147.51, 147.88($\underline{C}_6H_6$). ESI-MS. (Calcd, found, *m*/*z*): $[M + H]^+$ 383.1063, 383.1062.

L1, **L2**, and **L3** were synthesized by reaction of APBI with 2-chloro-7-methoxy-quinoline-3-carbaldehyde (**CMQC**), 2-chloro-6-methyl-quinoline-3-carbaldehyde, and 2-chloro-quinoline-3-carbaldehyde, respectively. Simple synthetic strategy adopted for the preparation of aldehydes and probes **L1-L3** is depicted in Scheme 1. All these were obtained in good yield (85-90%). The probes under investigation are non-hygroscopic, air-stable crystalline solids, highly soluble in common organic solvents like dichloromethane, chloroform, acetone, dimethylsulfoxide, acetonitrile, and partially soluble in methanol, ethanol.

Synthesis of L1–Fe^{3+}.

L1 (412 mg, 1 mmol) and ferric nitrate nonahydrate (202 mg, 0.5 mmol) were mixed in equimolecular ratio in 1:1 CH_3CN:H_2O mixture, and stirred overnight to ensure complete reaction. The solvent was dried and the residue was washed several times with water and diethyl ether. The dried sample was used for further characterization.

Hydrolysis of L1 in presence of Hg^{2+}. The adapted procedure for the hydrolysis of **L1** (342.62 mg, 1 mmol) was same as for **L1–Fe^{3+}**. After thorough washing with water and diethyl ether, dried sample was used for further characterizations.

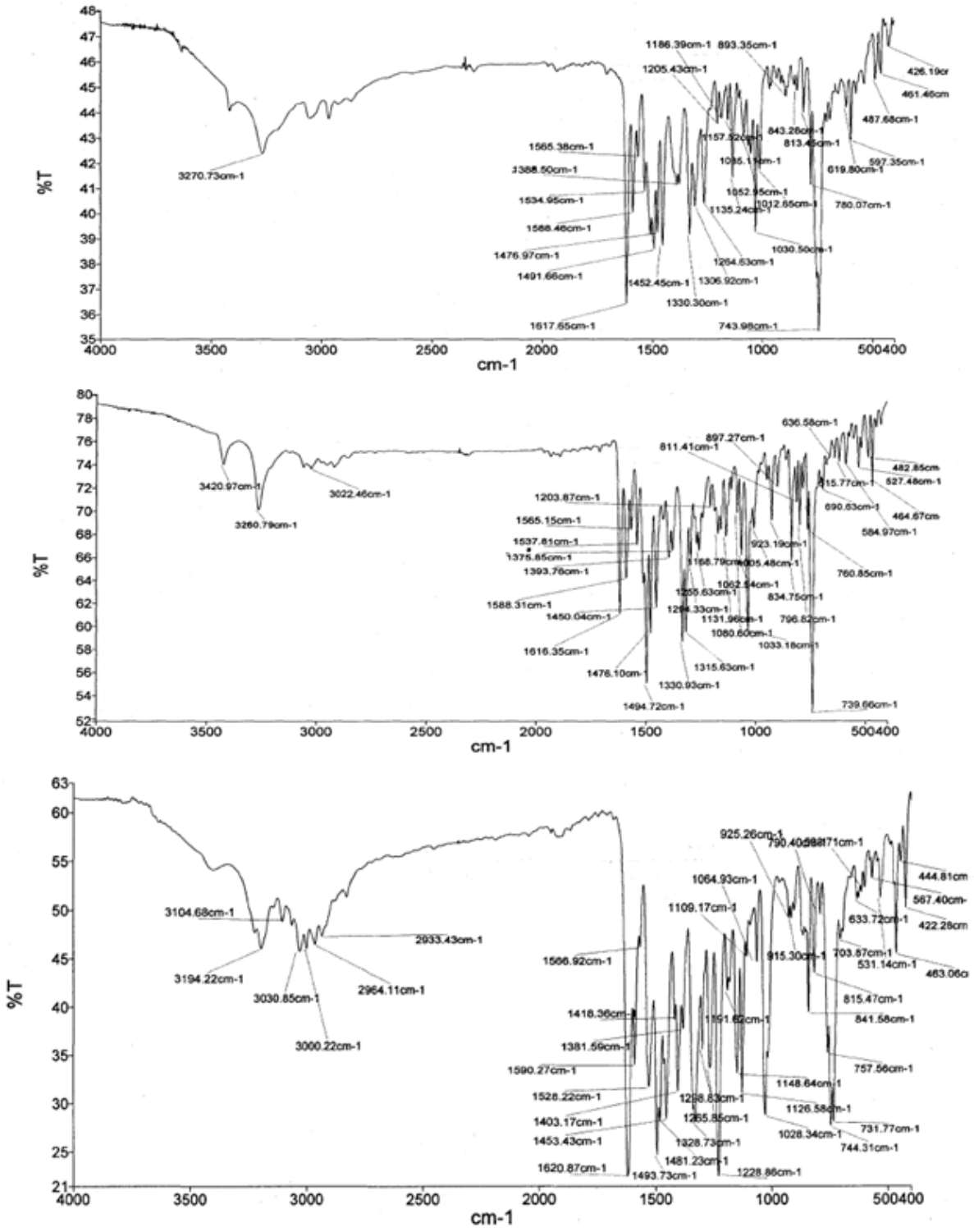

Figure S1. IR spectra of **L1**–**L3**.

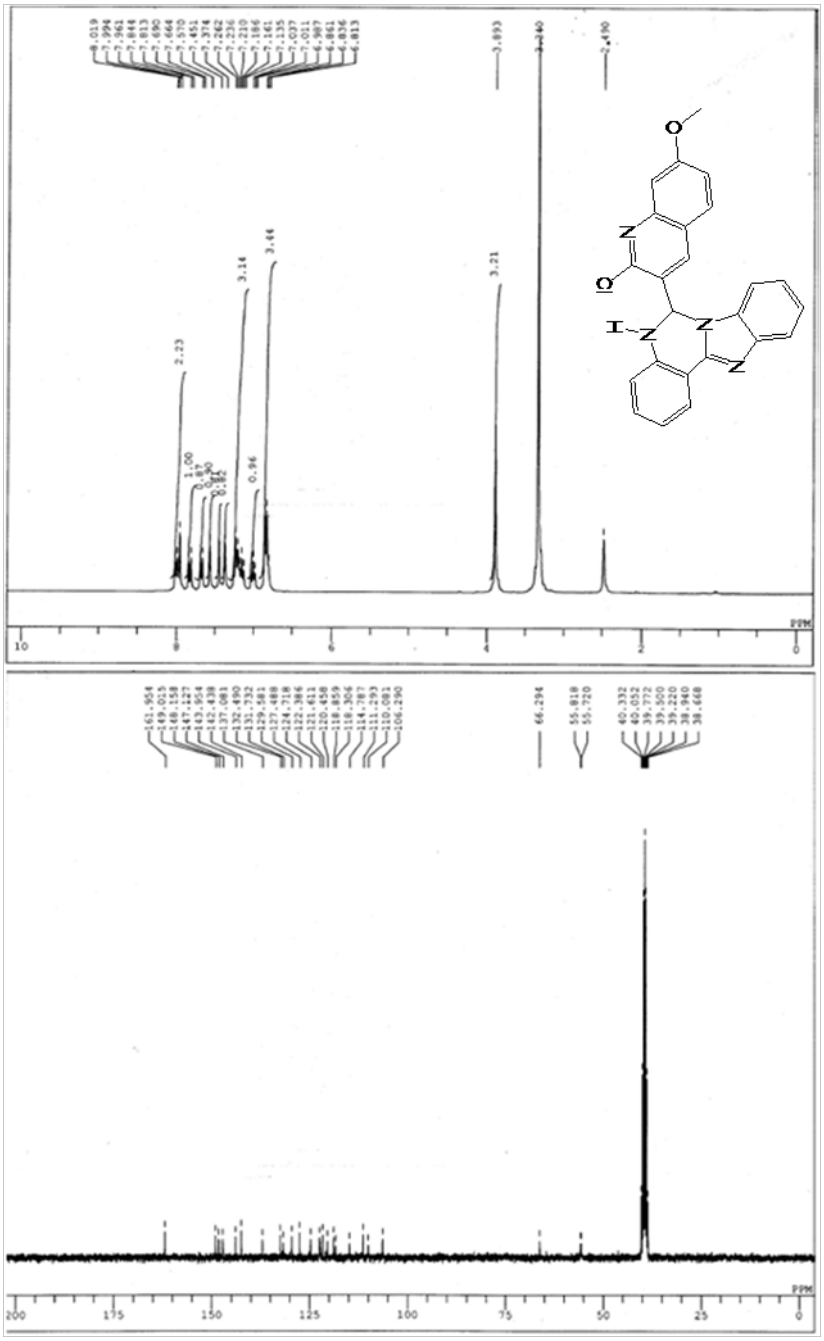

Figure S2. ^{1}H and ^{13}C NMR spectra of **L1**.

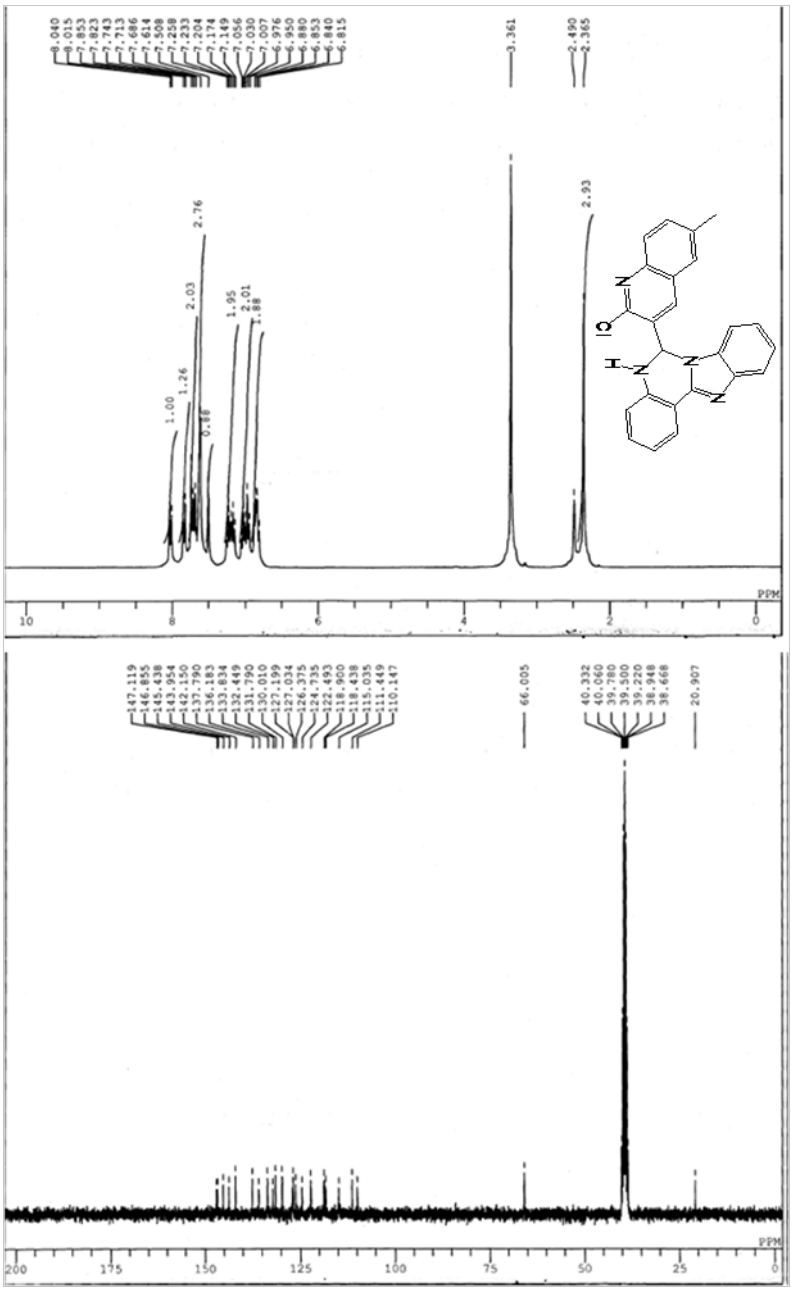

Figure S3. ^{1}H and ^{13}C NMR spectra of **L2**.

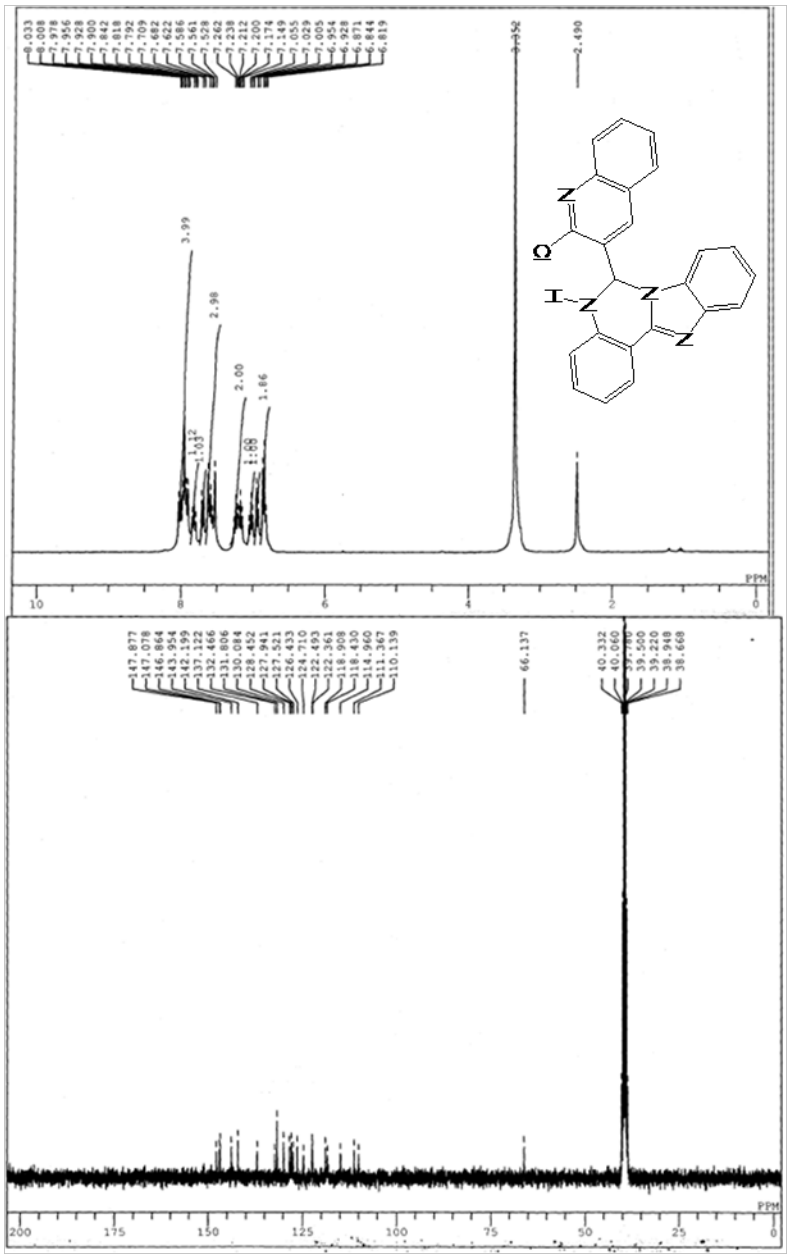

Figure S4. ^{1}H and ^{13}C NMR spectra of **L3**.

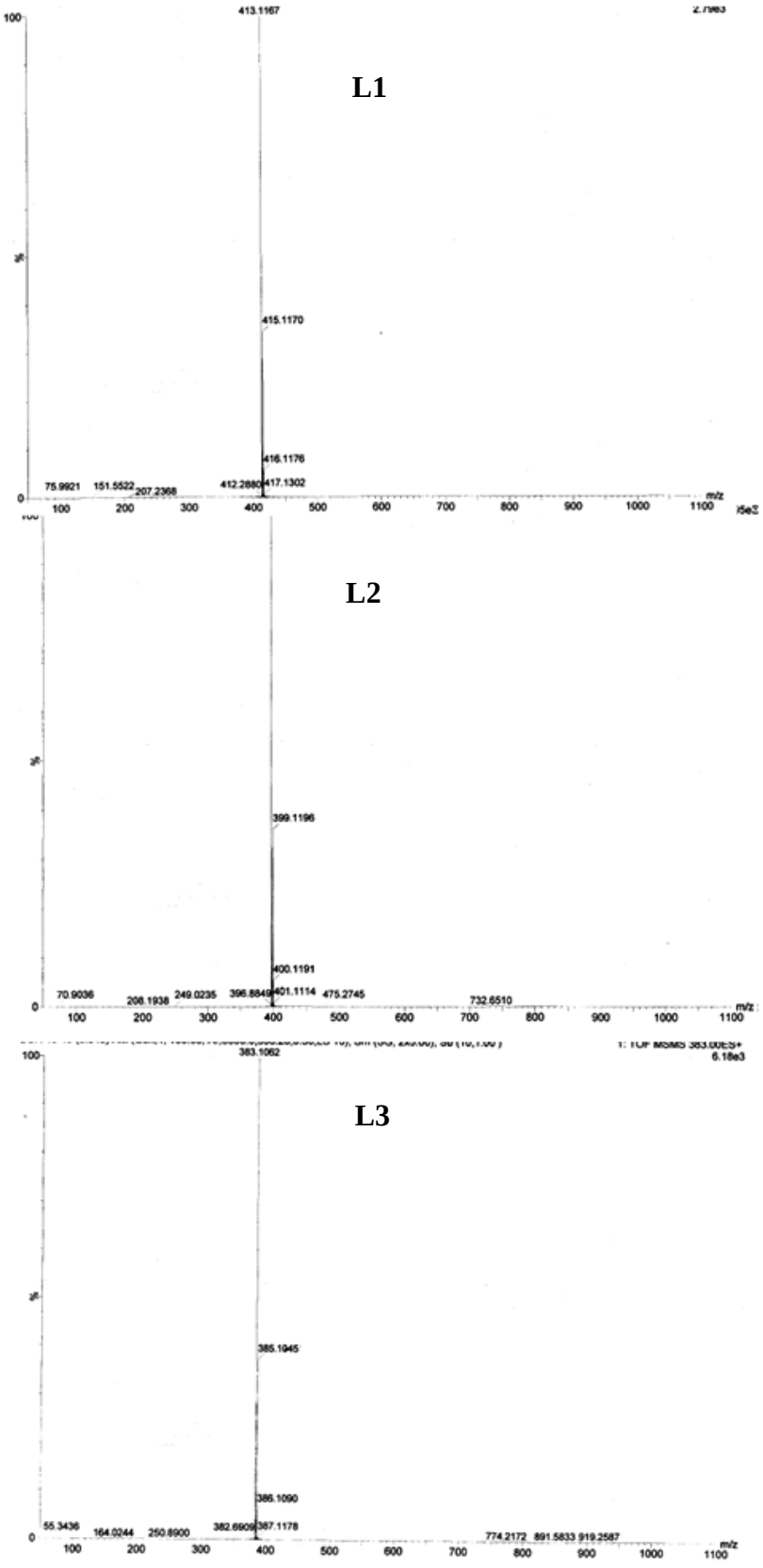

Figure S5. ESI-MS spectra of **L1-L3**.

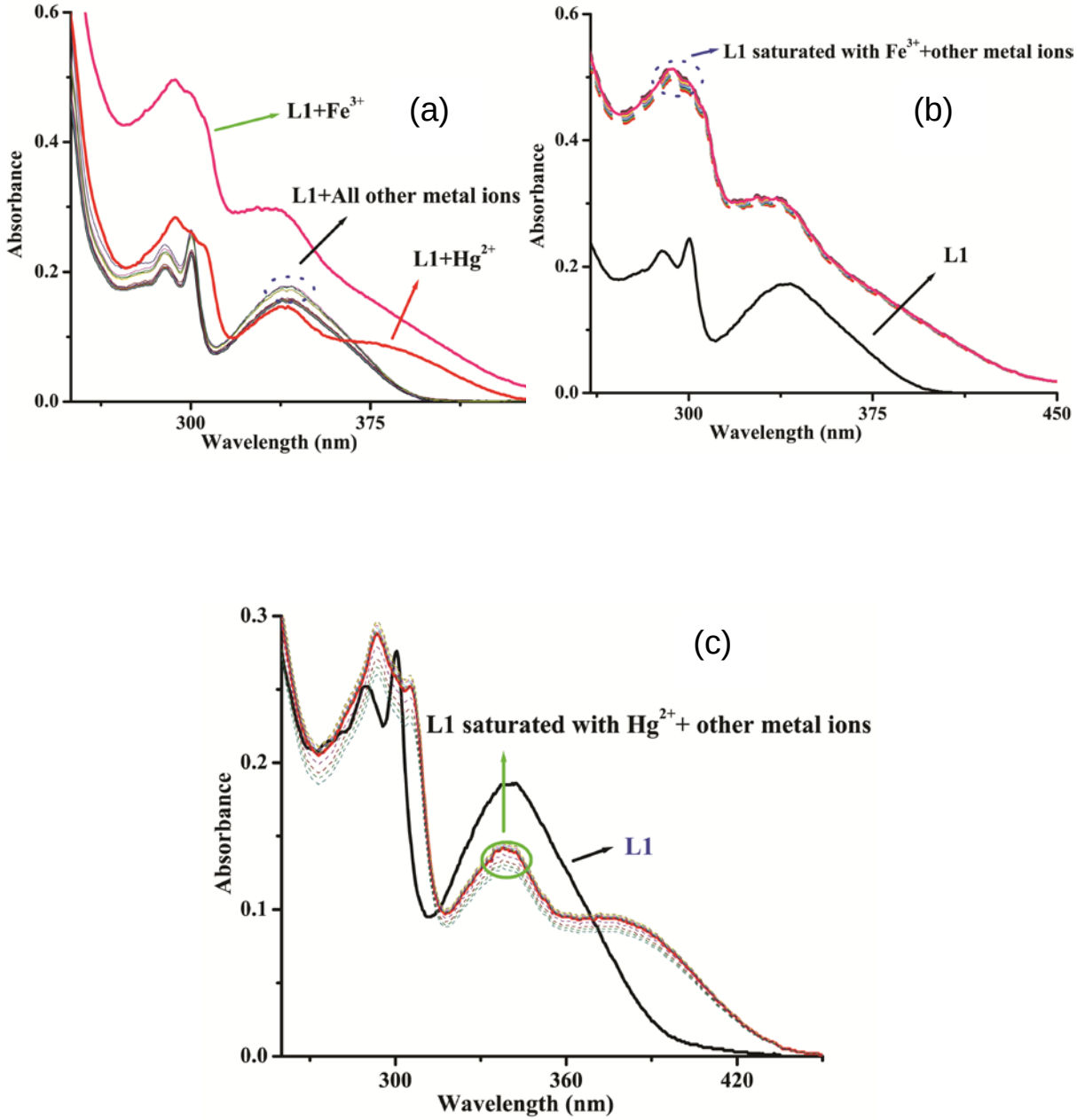

Figure S6. Sensing behavior of **L1** by UV–vis spectroscopy for (a) individual metal ions (Fe^{3+}, Na^{+}, K^{+}, Ca^{2+}, Mg^{2+}, Mn^{2+}, Ni^{2+}, Al^{3+}, Co^{2+}, Zn^{2+}, Cu^{2+}, Cd^{2+}, and Hg^{2+}.). (b) and (c) interference of other metal ions in saturated solution of **L1**–Fe^{3+} (Na^{+}, K^{+}, Mg^{2+}, Ca^{2+}, Mn^{2+}, Ni^{2+}, Al^{3+}, Co^{2+}, Zn^{2+}, Cu^{2+}, Cd^{2+}) and **L1**–Hg^{2+}, respectively.

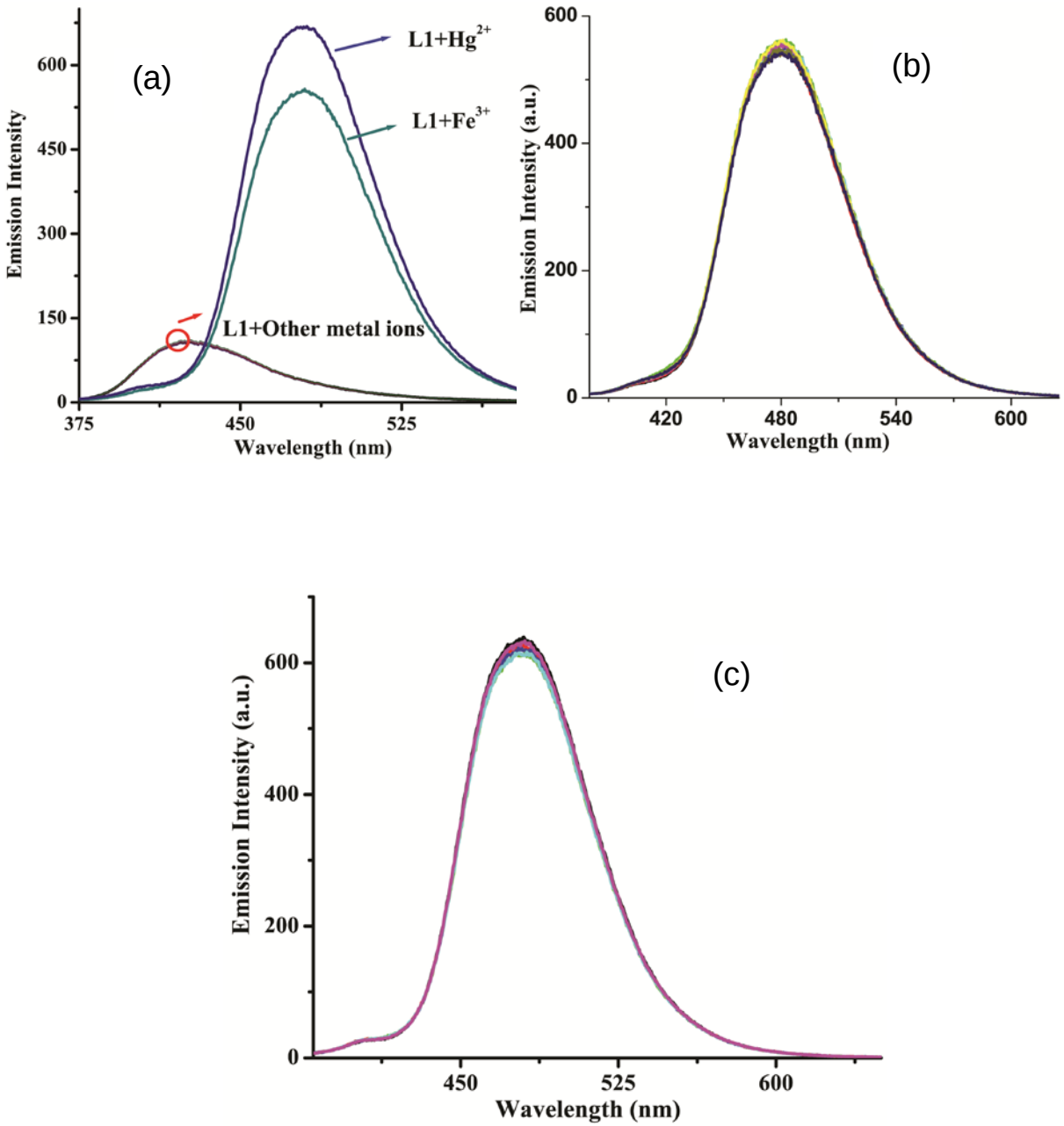

Figure S7. (a) Individual metal ion (Fe^{3+}, Na^{+}, K^{+}, Ca^{2+}, Mg^{2+}, Mn^{2+}, Ni^{2+}, Al^{3+}, Co^{2+}, Zn^{2+}, Cu^{2+}, Cd^{2+}, and Hg^{2+}) sensing behavior of **L1** by fluorescence spectroscopy. (b) and (c) Interference of other metal ions in the saturated solution of **L1**-Fe^{3+} (Na^{+}, K^{+}, Mg^{2+}, Ca^{2+}, Mn^{2+}, Ni^{2+}, Al^{3+}, Co^{2+}, Zn^{2+}, Cu^{2+}, Cd^{2+}) and **L1**-Hg^{2+} respectively.

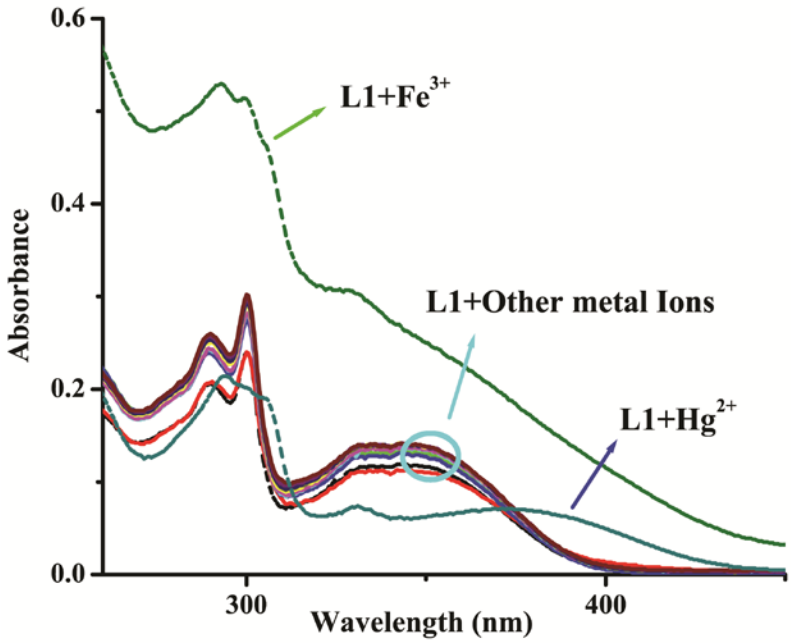

Figure S8. Individual metal ion (Fe^{3+}, Na^{+}, K^{+}, Ca^{2+}, Mg^{2+}, Mn^{2+}, Ni^{2+}, Al^{3+}, Co^{2+}, Zn^{2+}, Cu^{2+}, Cd^{2+}, and Hg^{2+}.) sensing behavior of **L2** by UV–vis spectroscopy.

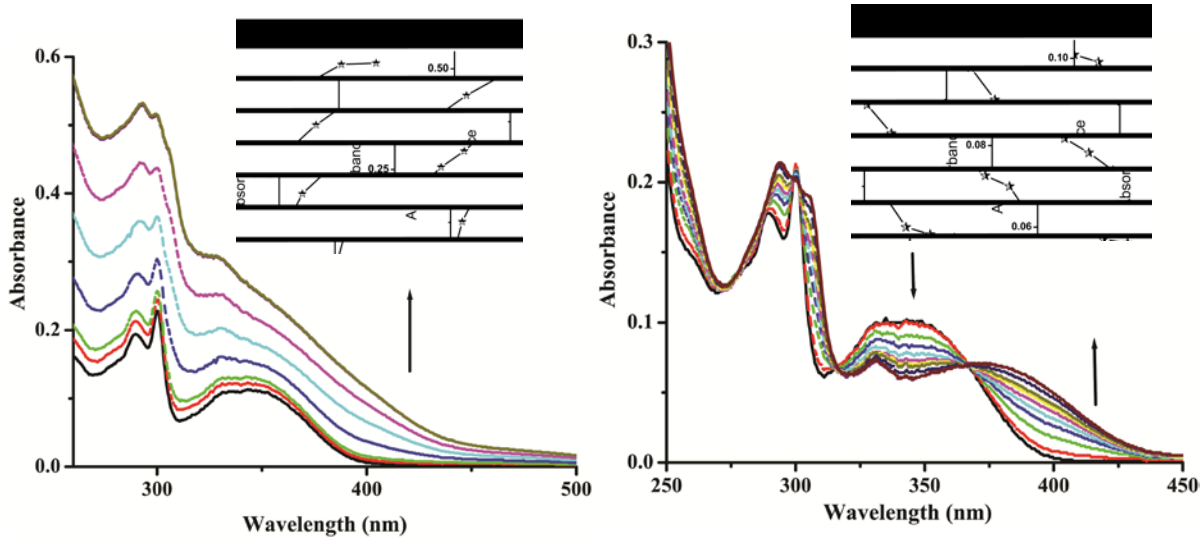

(a) (b)

Figure S9. (a) UV–vis titration of **L2** with 6.0 equiv of Fe^{3+}. (b) UV–vis titration of **L2** with 3.0 equiv of Hg^{2+}. Insets are showing changes in absorbance at 340 nm with changes in concentration of Fe^{3+} and Hg^{2+}.

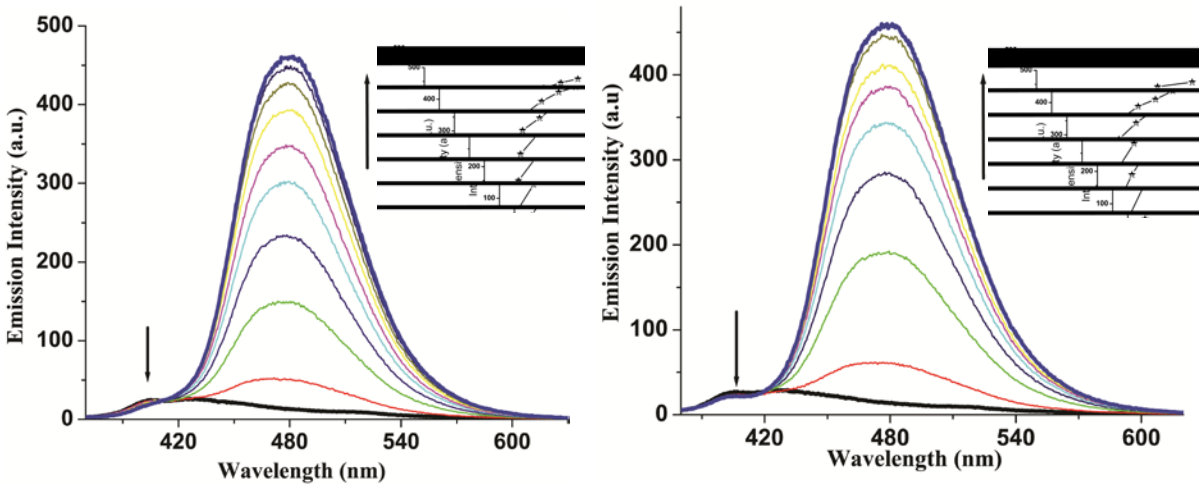

(a) (b)

Figure S10. (a) Fluorescence titration of **L2** with 6.0 equiv of Fe^{3+}. (b) 3.0 equiv of Hg^{2+}. Insets are showing changes in intensity at 480 nm with changes in concentration of Fe^{3+} and Hg^{2+}.

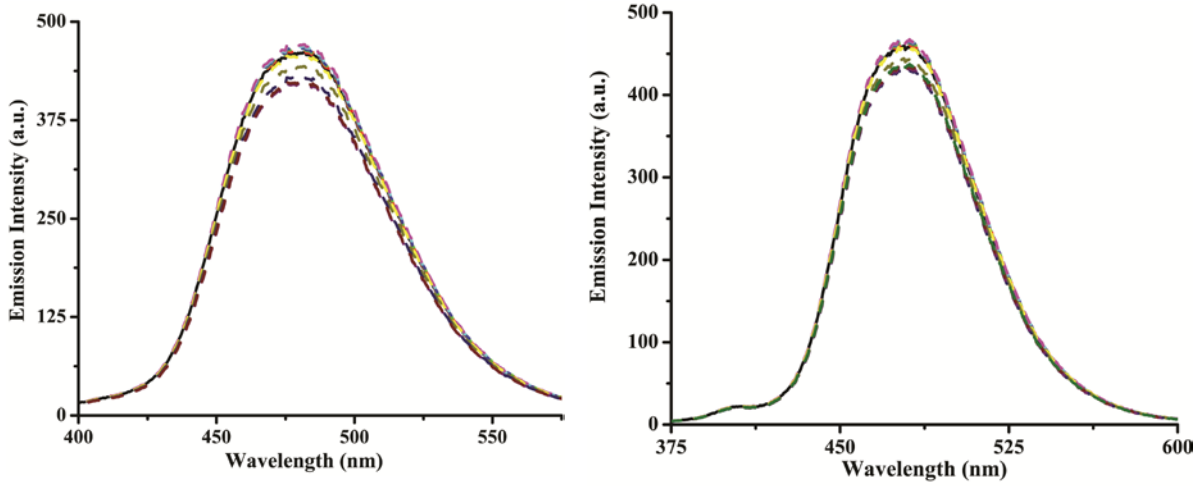

(a) (b)

Figure S11. (a) and (b) Interference of other metal ions in the saturated solution of **L2**-Fe^{3+} (Na^{+}, K^{+}, Mg^{2+}, Ca^{2+}, Mn^{2+}, Ni^{2+}, Al^{3+}, Co^{2+}, Zn^{2+}, Cu^{2+}, Cd^{2+}) and **L2**-Hg^{2+} respectively.

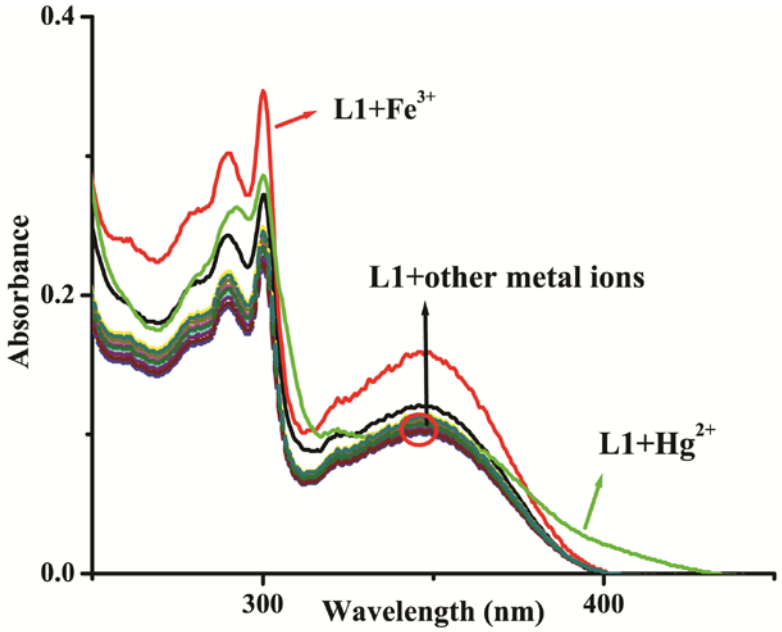

Figure S12. Individual metal ion (Fe^{3+}, Na^{+}, K^{+}, Ca^{2+}, Mg^{2+}, Mn^{2+}, Ni^{2+}, Al^{3+}, Co^{2+}, Zn^{2+}, Cu^{2+}, Cd^{2+}, and Hg^{2+}.) sensing behavior of **L3** by UV–vis spectroscopy.

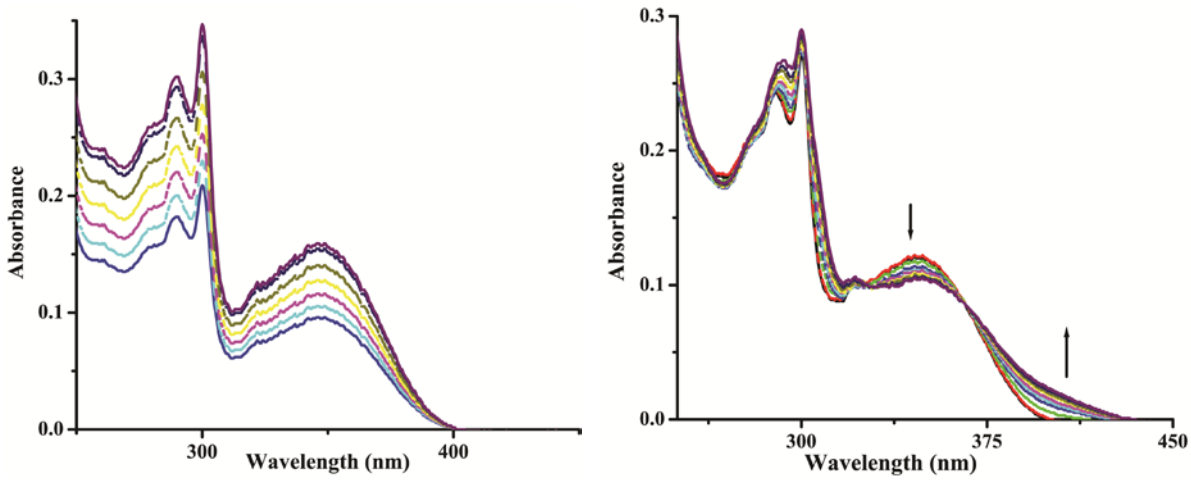

(a) (b)

Figure S13. (a) UV–vis titration of **L3** with 6.0 equiv of Fe^{3+}. (b) UV–vis titration of **L3** with 3.0 equiv of Hg^{2+}.

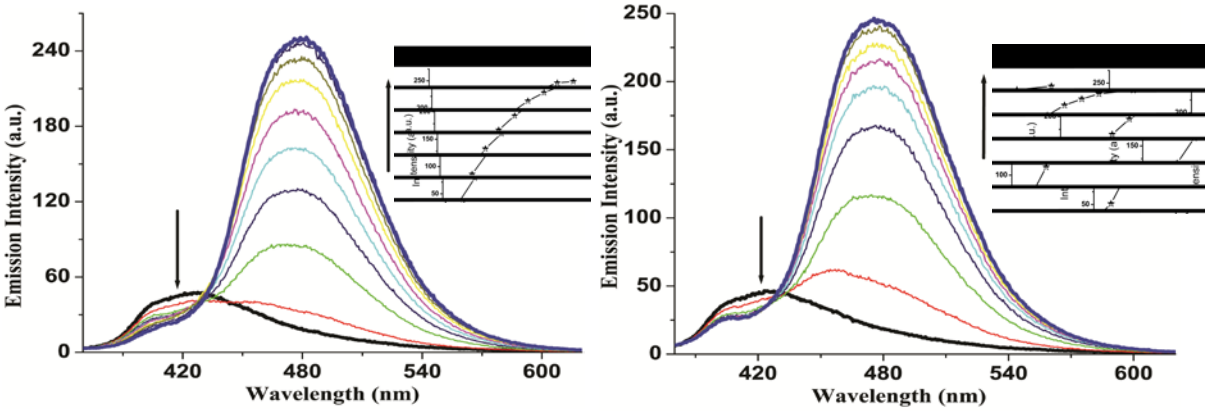

Figure S14. (a) Fluorescence titration of **L3** with 6.0 equiv of Fe^{3+}. (b) Fluorescence titration of **L3** with 3.0 equiv of Hg^{2+}. Insets are showing changes in intensity at 480 nm with changes in concentration of Fe^{3+} and Hg^{2+}.

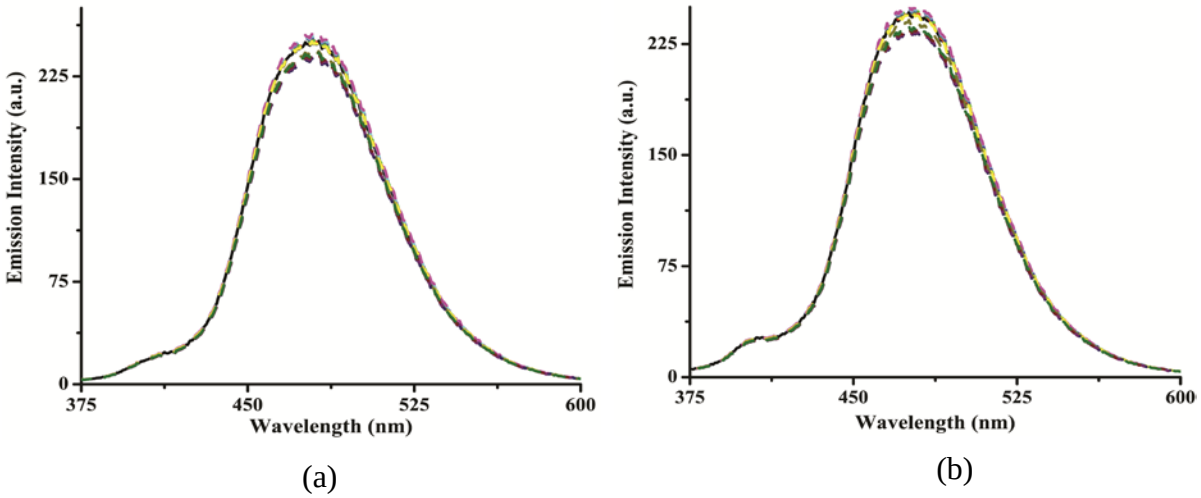

Figure S15. (a) And (b) Interference of other metal ions in the saturated solution of **L3**-Fe^{3+} (Na^{+}, K^{+}, Mg^{2+}, Ca^{2+}, Mn^{2+}, Ni^{2+}, Al^{3+}, Co^{2+}, Zn^{2+}, Cu^{2+}, Cd^{2+}) and **L3**-Hg^{2+} respectively.

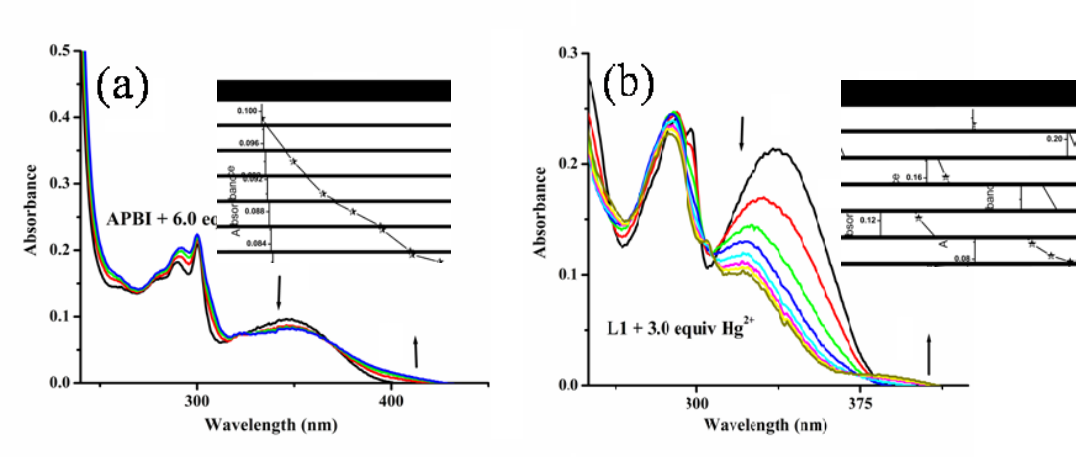

Figure S16. UV–vis titration spectra of **APBI** with (a) Fe^{3+} and (b) Hg^{2+}. Insets are showing changes in absorbance at 340 nm with changes in concentration of Fe^{3+} and Hg^{2+}.

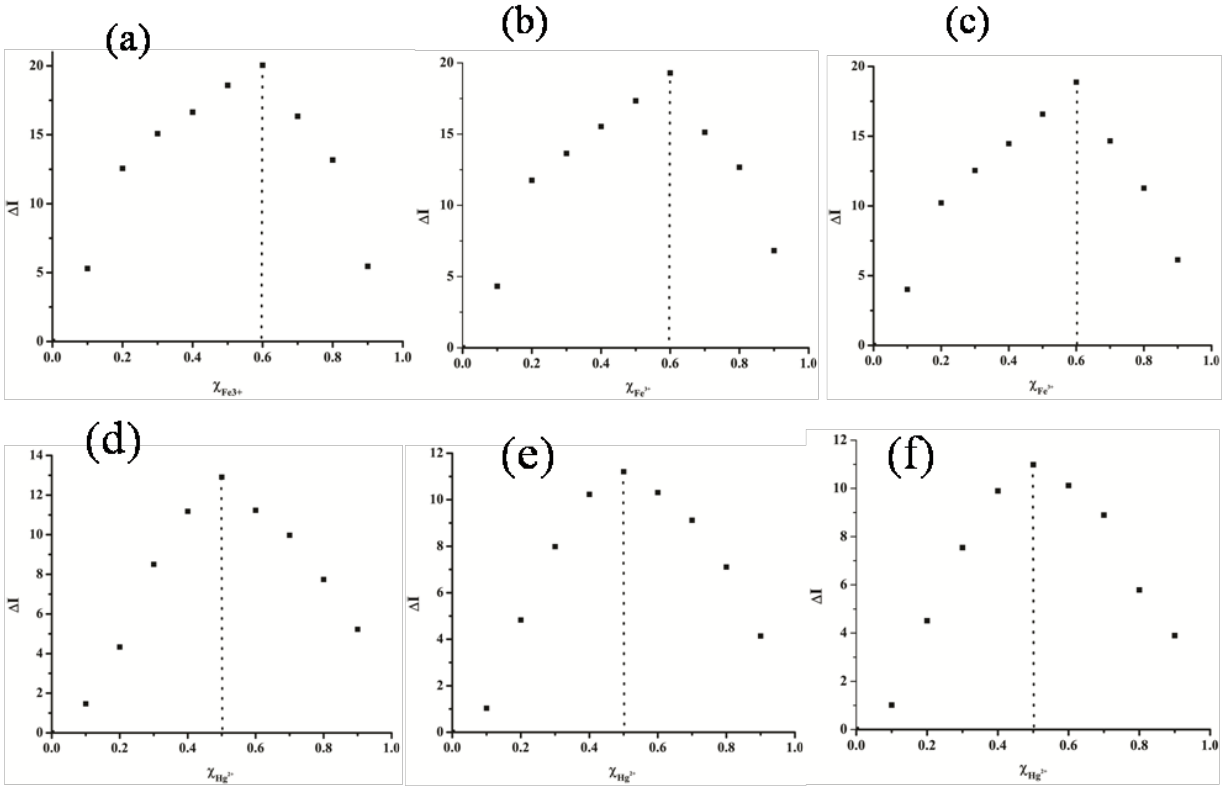

Figure S17. Job's plot showing 1:2 stoichiometries of Fe^{3+} with (a) **L1**, (b) **L2**, (c) **L3**. Job's plot showing 1:1 stoichiometries of Hg^{2+} with (d) **L1**, (e) **L2**, (f) **L3**.

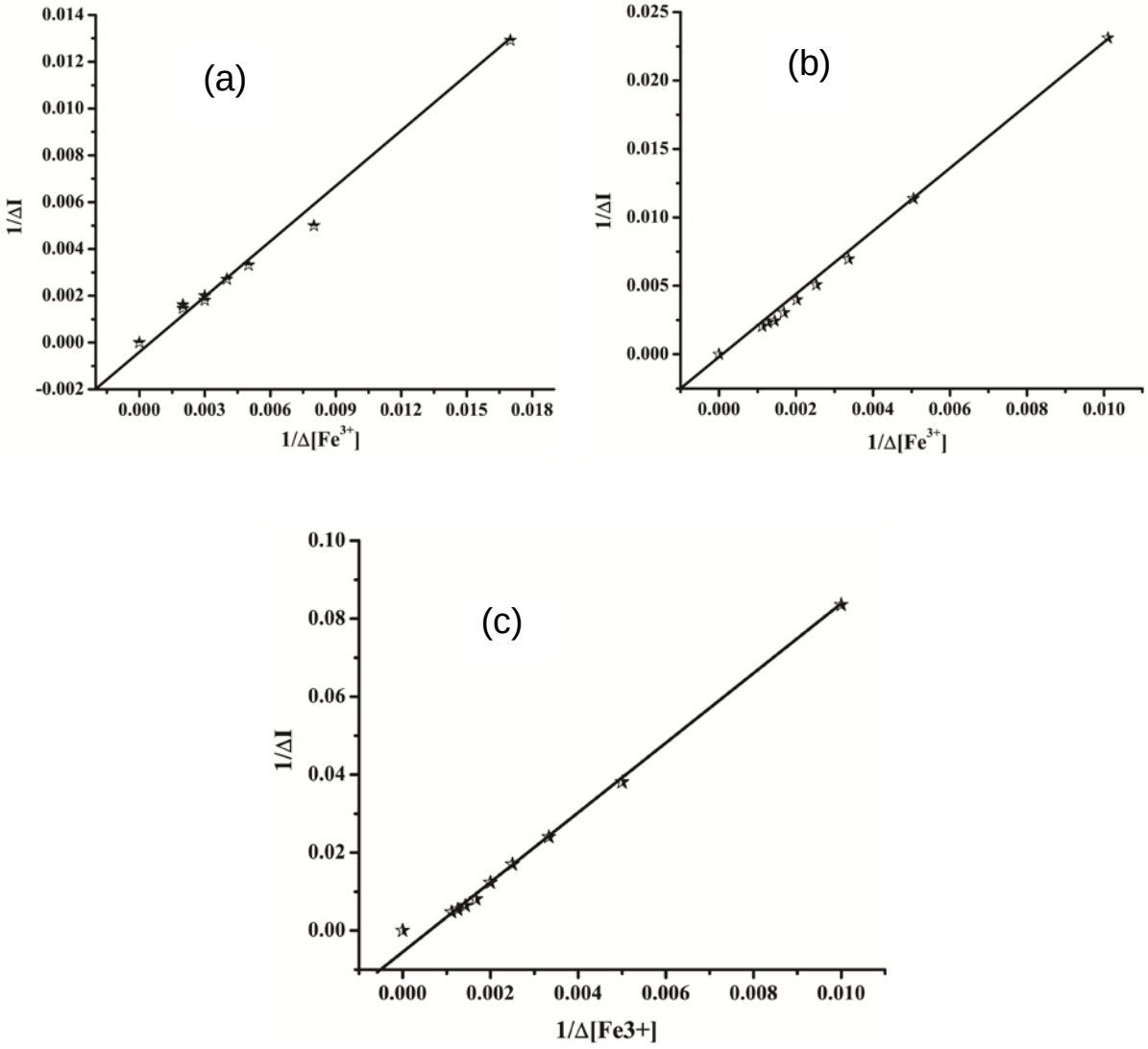

Figure S18. Benesi Hildebrand plot of (a) **L1**, (b) **L2**, (c) **L3**.

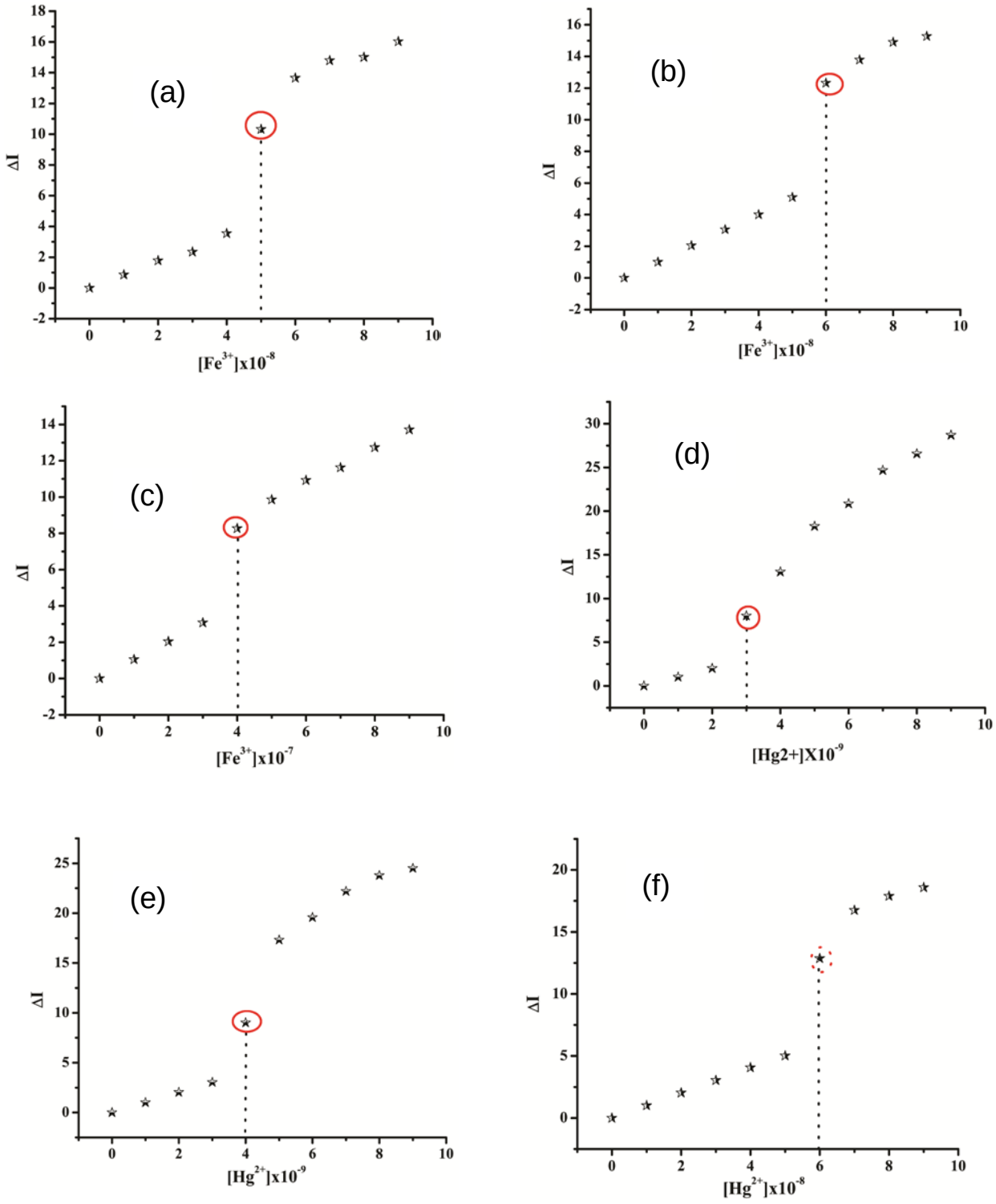

Figure S19. Plot of $\Delta(I\text{-}I_0)$ *vs.* $[Fe^{3+}]$ with [**L**] = 10 μM for the calculation of lowest detection limit: LOD for Fe^{3+} has been calculated by standard analytical method using equation $3\sigma/s$ and found to be (a) 18.5 ppb for **L1**, (b) 20.4 ppb for **L2**, (c) 109.67 ppb for **L3**. LOD for Hg^{2+} has been calculated by standard analytical method using equation $3\sigma/s$ and found to be (d) 1.98 ppb for **L1**, (e) 2.27 ppb for **L2**, (f) 13.33 ppb for **L3**.

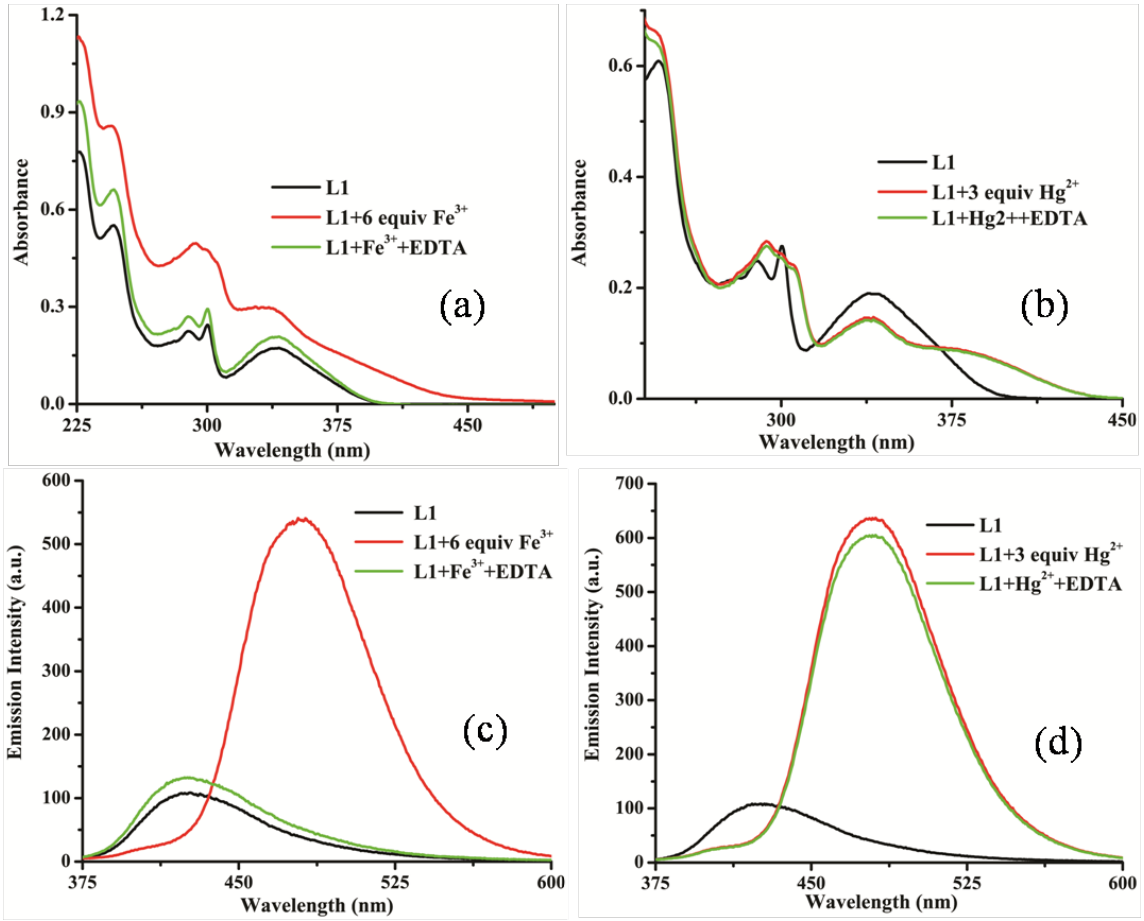

Figure S20. (a) UV–vis spectra of **L1** (10 μM) with Fe^{3+} (10^{-1}M) and excess EDTA (10 mM). (b) UV–vis spectra of **L1** (10 μM) with Hg^{2+} (10^{-2}M) and excess EDTA (10 mM). (c) Fluorescence spectra of **L1** (10 μM) with Fe^{3+} (10^{-1}M) and excess EDTA (10 mM). (d) Fluorescence spectra of **L1** (10 μM) with Hg^{2+} (10^{-1}M) and excess EDTA (10 mM).

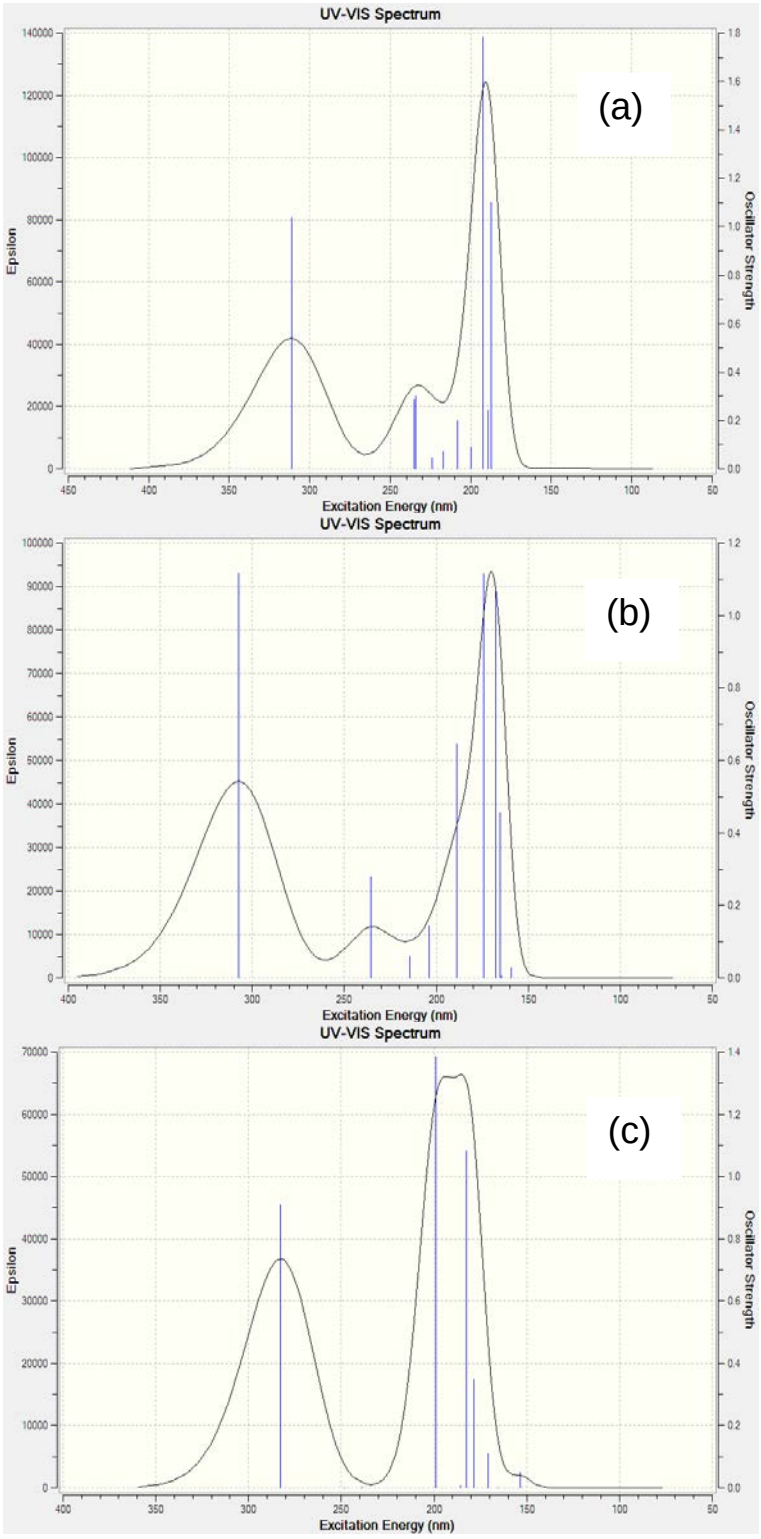

Figure S21. Theoretically calculated (by TDDFT) UV-vis spectra of (a) **L1**, (b) **APBI**, and (c) **CMQC**.

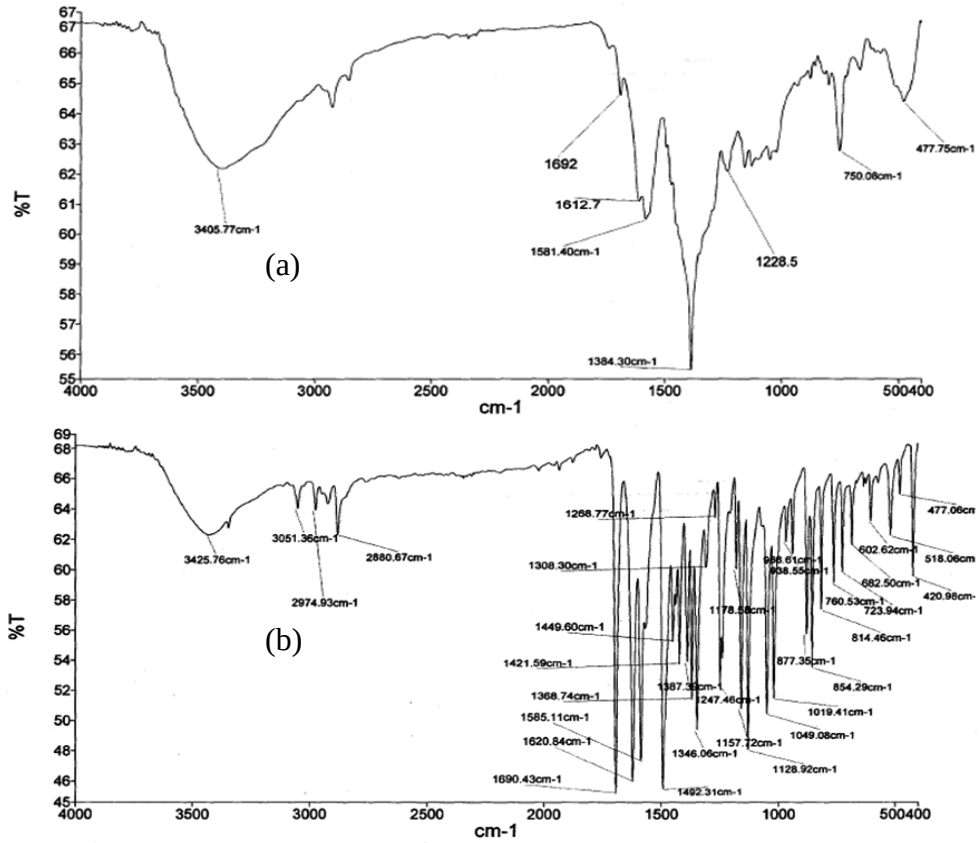

Figure S22. (a) IR spectra of **L1**-Fe^{3+}, (b) Hg^{2+} induced hydrolyzed product.

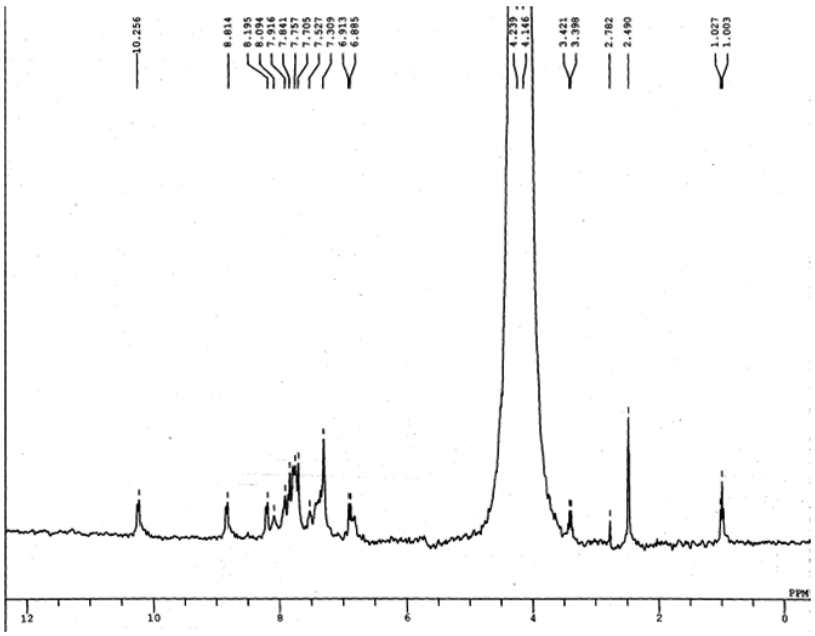

Figure S23. 1H NMR spectra of Hg^{2+} induced hydrolyzed product.

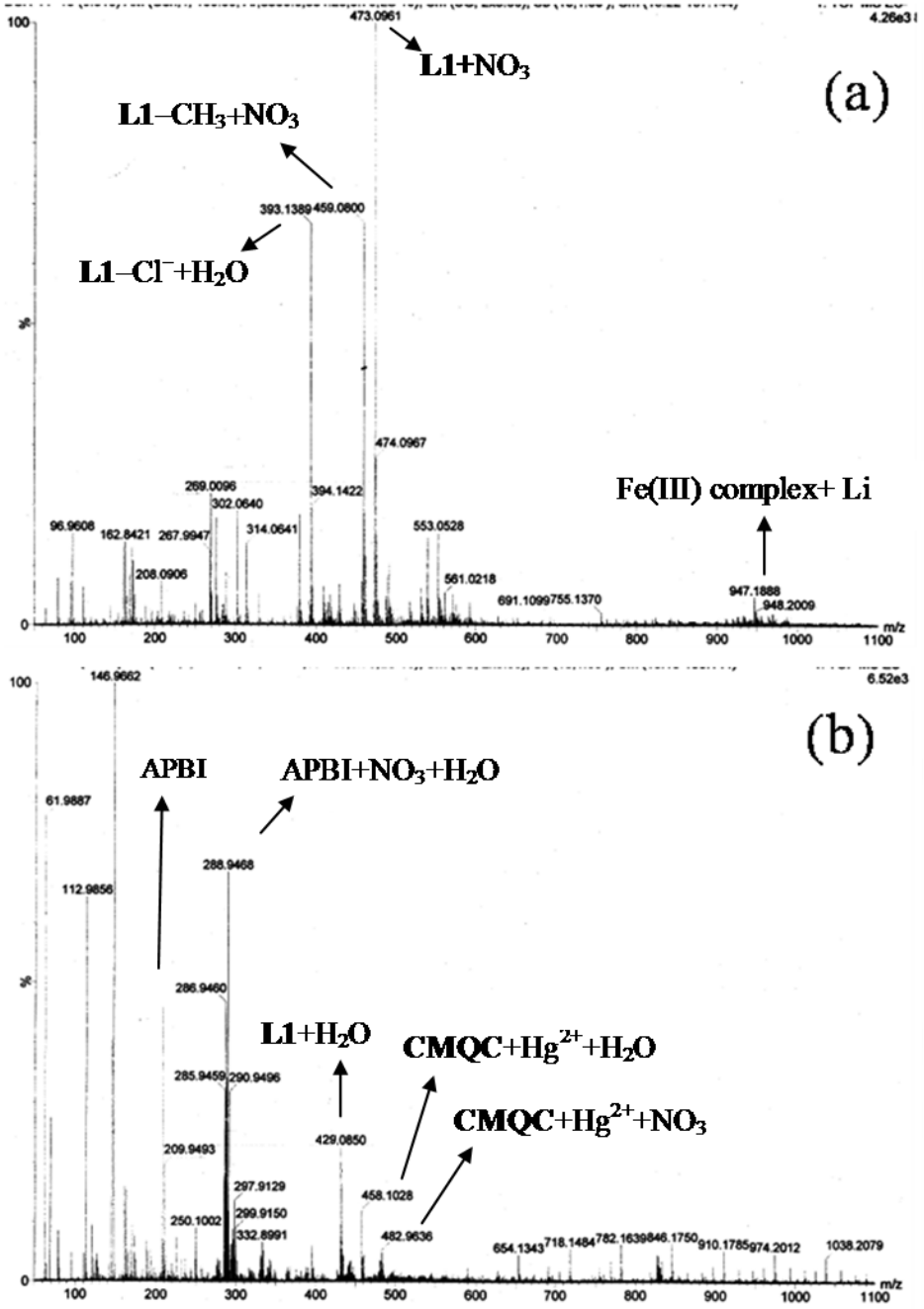

Figure S24. (a) ESI-Mass spectra of L1-Fe^{3+}, (b) Hg^{2+} induced hydrolyzed product.

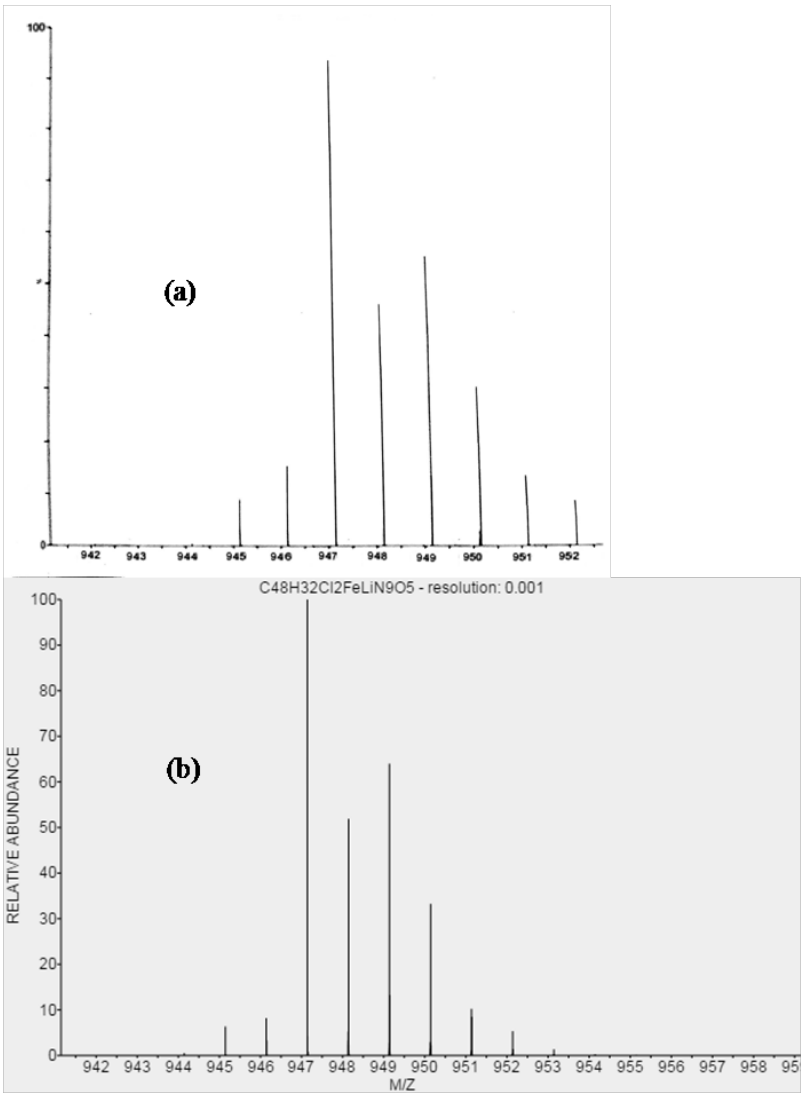

Figure S25. Isotopic mass spectral pattern of L1–Fe^{3+} (a) found and (b) calculated.

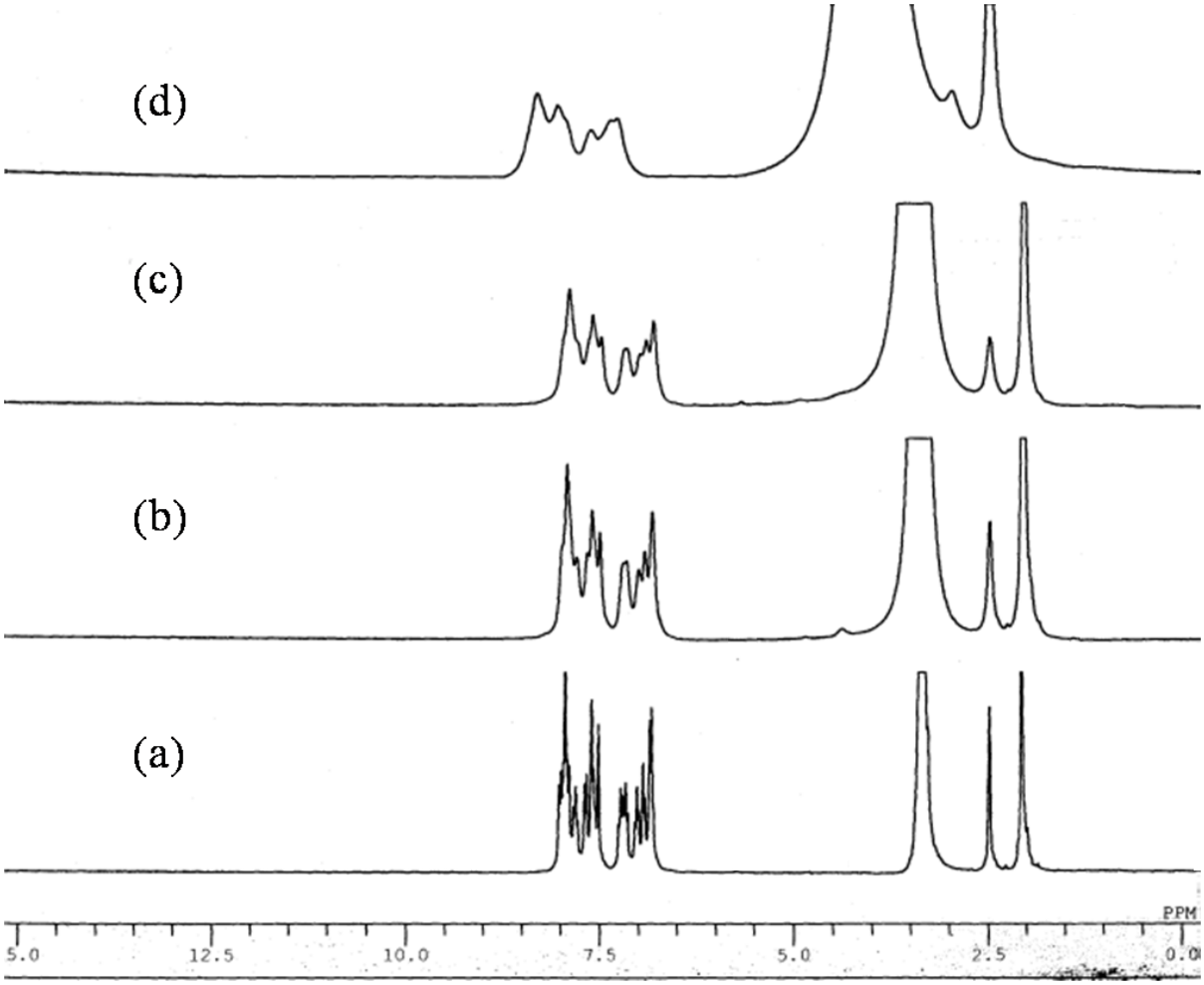

Figure S26. ^{1}H NMR spectral titration of **L1** with various amount of (a) Fe^{3+} 0.0 equiv, (b) 0.50 equiv, (c)1.0 equiv, and (d) 2.0 equiv.

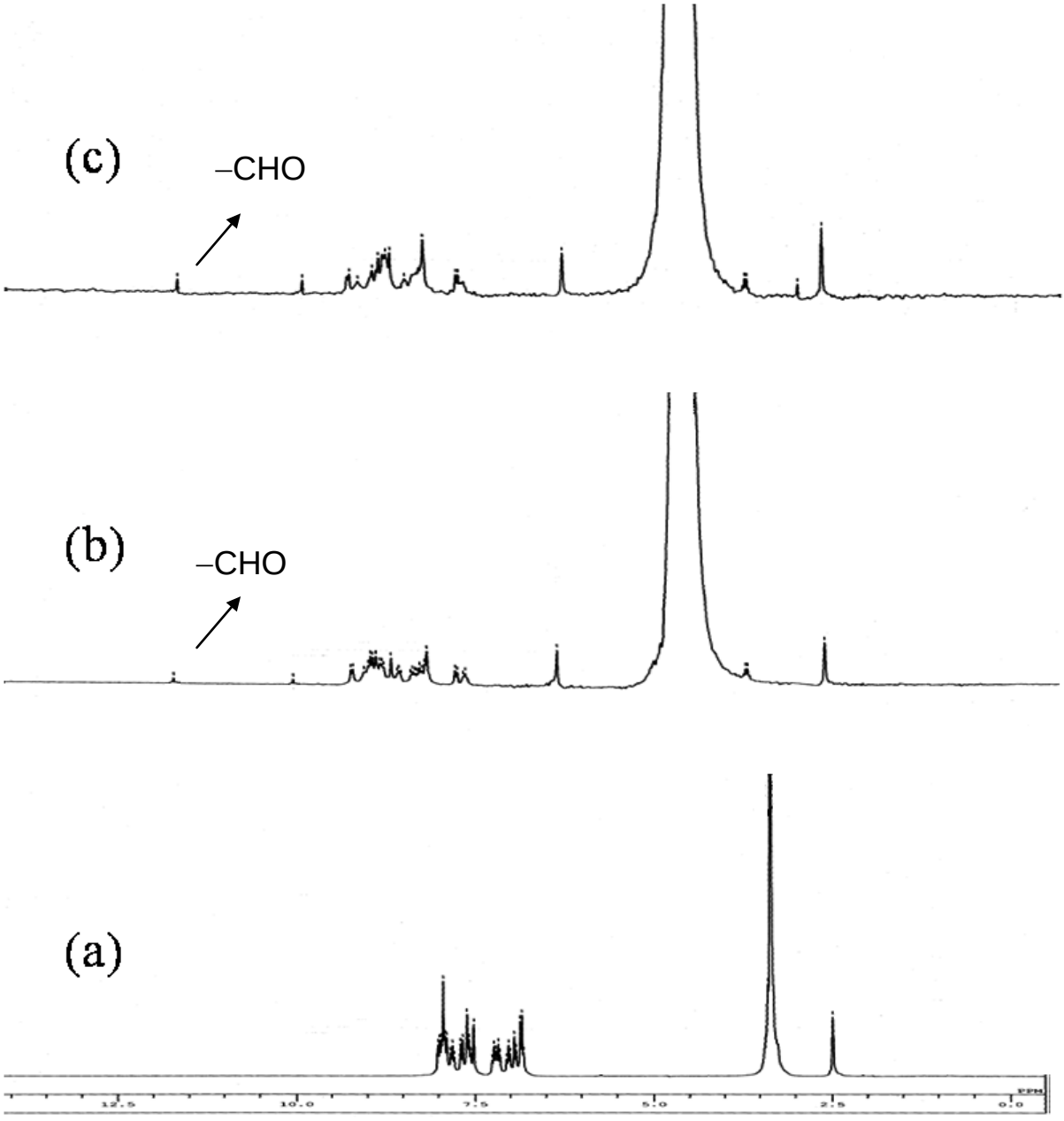

Figure S27. ^{1}H NMR spectral titration of **L1** with various amount of (a) Hg^{2+} 0.0 equiv, (b) 0.50 equiv, (c) 1.0 equiv.

References:

1 D. D. Perrin, W. L. F. Armango and D. R. Perrin, *Purification of laboratory Chemicals*, Pergamon, Oxford, UK, 1986.

2 L. J. Bartolottiand and K. Fluchick, *In Reviews in Computational Chemistry*; K. B. Lipkowitz and D. Boyd, Ed. VCH: New York, 1996, **7**, 187.

3 G. M. Sheldrick, SHELXL-97, Program for X-ray Crystal Structure Refinement; Göttingen University: Göottingen, Germany, (1997); G. M. Sheldrick, SHELXS-97, Program for X-ray Crystal Structure Solution; Göttingen University: Göttingen, Germany, (1997).

4 A. L.Spek, PLATON, A Multipurpose Crystallographic Tools; Utrecht University, Utrecht, The Netherlands, (2000); A. L. Spek, Acta Crystallogr. A 1990, **46**, C31.

5 M. J. Frisch, G. W. Trucks, H. B. Schlegel, G. E. Scuseria, M. A. Robb, J. R. Cheeseman, G. Scalmani, V. Barone, B. Mennucci, G. A. Petersson, H. Nakatsuji, M. Caricato, X. Li, H. P. Hratchian, A. F. Izmaylov, J. Bloino, G. Zheng, J. L. Sonnenberg, M. Hada, M. Ehara, K. Toyota, R. Fukuda, J. Hasegawa, M. Ishida, T. Nakajima, Y. Honda, O. Kitao, H. Nakai, T. Vreven, J. A. Jr. Montgomery, J. E. Peralta, F. Ogliaro, M. Bearpark,; J. J. Heyd, E. Brothers, K. N. Kudin, V. N. Staroverov, R. Kobayashi, J. Normand, K. Raghavachari, A. Rendell, J. C. Burant, S. S. Iyengar, J. Tomasi, M. Cossi, N. Rega, N. J. Millam, M. Klene, J. E. Knox, J. B. Cross, V. Bakken, C. Adamo, J. Jaramillo, R. Gomperts, R. E. Stratmann, O. Yazyev, A. J. Austin, R. Cammi, C. Pomelli, J. W. Ochterski, R. L. Martin, K. Morokuma, V. G. Zakrzewski, G. A. Voth, P. Salvador, J. J. Dannenberg, S. Dapprich, A. D. Daniels, Ö. Farkas, J. B. Foresman, J. V. Ortiz, J. Cioslowski and D. J. Fox, *Gaussian, Inc., Wallingford CT*, 2009.

6 (*a*) P. Hay and W. R. Wadt, *J. Chem. Phys*., 1985, **82**, 270; (*b*) W. R. Wadt and P. Hay, *J. Chem. Phys.*, 1985, **82**, 284; (*c*) P. Hay and W. R. Wadt, *J. Chem. Phys*., 1985, **82**, 299.

7 Y. Zhang, Y. Fang, H. Liang, H. Wang, K. Hu, X. Liu, X. Yi, Y. Peng, *Bioorg. Med. Chem. Lett.* 2013, **23**, 107–111.

Table S1. Crystal data and structure refinement parameters for **L1**, **L2** and **L3**

Crystal parameters	**L1**	**L2**	**L3**	**CMQC**
Empirical formula	$C_{24}H_{17}ClN_4O$	$C_{24}H_{17}ClN_4$	$C_{23}H_{15}ClN_4$	$C_{11}H_8ClNO_2$
Formula weight	412.87	428.91	414.88	221.63
Crystal system	Monoclinic	Monoclinic	Triclinic	Monoclinic
Space group	*P* $2_1/n$	*P* $2_1/c$	*P -1*	*P* $2_1/n$
a (Å)	13.029(2)	12.708(3)	9.363(13)	3.827(6)
b (Å)	22.884(5)	18.351(3)	9.516(16)	29.579(4)
c (Å)	13.417(3)	9.062(17)	12.620(2)	8.624(12)
α (deg)	90.00	90.00	85.85(7)	90.00
β (deg)	92.34(6)	92.62(6)	86.13(7)	95.35(7)
γ (deg)	90.00	90.00	80.74(7)	90.00
V ($Å^3$)	3997.0 (14)	2111.0 (7)	1105.1 (3)	972.1 (2)
Color and habit	Prism, white	Needles, colorless	Rectangular, colorless	Block, white
Z	8	4	2	4
dcal (g/cm^3)	1.372	1.350	1.247	1.514
Temperature (K)	296(2)	296(2)	296(2)	296(2)
wavelength (Å)	0.71073	0.71073	0.71073	0.71073
μ (mm^{-1})	0.215	0.206	0.195	0.368
GOF on F^2	0.937	1.020	1.027	1.032
R indices (All data)	R1 = 0.2247 wR2 = 0.1870	R1 = 0.1545 wR2 = 0.2381	R1 = 0.1157 wR2 = 0.3013	R1 = 0.0931 wR2= 0.2030
final R indices [I > 2σ(I)]	R1 = 0.0667 wR2 = 0.1343	R1 = 0.0703 wR2 = 0.1875	R1 = 0.0882 wR2 = 0.2696	R1 = 0.0620 wR2= 0.1784

Table S2. Selected bond length of **L1**, **L2** and **L3**.

Bond length (Å)	L1	Bond length (Å)	L2	Bond length (Å)	L3
C1–N1	1.432(5)	C1–N1	1.371(5)	C1–N1	1.369(4)
C6–N2	1.417(5)	C9–N1	1.295(5)	C9–N1	1.291(4)
C7–N2	1.436(5)	C10–N2	1.438(5)	C10–N4	1.443(4)
C7–N3	1.475(5)	C10–N4	1.466(6)	C10–N2	1.446(4)
C9–N4	1.303(5)	C11–N2	1.415(6)	C11–N2	1.384(4)
C10–N4	1.367(5)	C16–N3	1.441(6)	C16–N3	1.404(5)
C18–N3	1.387(5)	C17–N3	1.297(6)	C17–N3	1.312(4)
C24–N1	1.305(5)	C17–N2	1.344(6)	C17–N2	1.370(4)
C24–N2	1.362(5)	C23–N4	1.413(6)	C23–N4	1.381(5)
C9–Cl1	1.747(4)	C9–Cl1	1.743(4)	C9–Cl1	1.747(3)
C12–O1	1.374(5)				

Table S3. Selected bond angles for **L1**, **L2** and **L3**.

Bond Angle (°)	L1	Bond Angle (°)	L2	Bond Angle (°)	L3
C6–C1–N1	110.2(4)	N1–C1–C2	119.5(4)	N1–C1–C6	121.7(3)
C2–C1–N1	129.9(5)	N1–C1–C6	122.0(4)	N1–C1–C2	118.7(3)
C5–C6–N2	132.0(5)	N1–C9–C8	126.0(4)	N1–C9–C8	126.5(3)
C1–C6–N2	104.9(4)	N2–C10–N4	106.4(3)	N4–C10–N2	108.5(3)
N2–C7–N3	106.2(3)	N2–C10–C8	111.9(3)	N4–C10–C8	111.4(3)
N2–C7–C8	112.4(4)	N4–C10–C8	110.2(3)	N2–C10–C8	111.1(2)
N3–C7–C8	110.0(3)	C12–C11–N2	132.4(6)	N2–C11–C12	132.1(3)

N4–C9–C8	126.5(4)	C16–C11–N2	104.9(4)	N2–C11–C16	104.6(3)
N4–C10–C16	122.5(4)	N3–C17–N2	115.6(4)	C15–C16–N3	129.9(3)
N4–C10–C11	118.1(4)	N3–C17–C18	127.7(4)	C11–C16–N3	110.7(3)
N1–C24–N2	113.4(4)	N2–C17–C18	116.7(4)	N3–C17–N2	113.3(3)

Table S4. UV−vis spectroscopic data of **L1**-**L3**.

Probe	Wavelength (nm)	ε	Δε for **L**+Fe^{3+}	Δε for **L**+Hg^{2+}	Isosbestic points for **L**+Hg^{2+}(nm)
L1	340	0.173	0.127, Hyperchromism	0.027, Hypochromism	370, 315, 302
	300	0.244	0.236, Hyperchromism	0.033, Hypochromism	
L2	343	0.113	0.156, Hyperchromism	0.062, Hypochromism	367, 316, 302
	300	0.228	0.288, Hyperchromism	0.026, Hypochromism	
L3	349	0.121	0.038, Hyperchromism	0.016, Hypochromism	366, 324
	300	0.209	0.138, Hyperchromism	0.081, Hypochromism	

Table S5. Fluorescence spectroscopic data of **L1-L3**.

Probe	λ_{ex}(nm)	λ_{em}(nm)	$\Delta\lambda_{em}$ for Fe^{3+}(nm)	$\Delta\lambda_{em}$ for Hg^{2+}(nm)	ΔI for Fe^{3+}(nm)	ΔI for Hg^{2+}(nm)	$*\phi_{L1}-\phi_{Fe3+}$ (%)	$*\phi_{L1}-\phi_{Hg^{2+}}$ (%)
L1	340	425	53	55	443	560	25-76	25-90
L2	343	410	69	70	435	433	21-60	21-81
L3	349	420	59	56	203	205	18-53	18-69

$*\phi$ = Quantum yield